ELSEVIER

Journal of Alloys and Compounds 463 (2008) 516–521

Journal of ALLOYS AND COMPOUNDS

www.elsevier.com/locate/jallcom

Temperature-dependant non-catalytic growth of ultraviolet-emitting ZnO nanostructures on silicon substrate by thermal evaporation process

Ahmad Umar [a], S.H. Kim [a], J.H. Kim [a], A. Al-Hajry [b], Yoon Bong Hahn [a,*]

[a] *School of Semiconductor and Chemical Engineering and BK21 Centre for Future Research, Materials and Devices, Chonbuk National University, Chonju, South Korea*

[b] *Department of Physics, College of Science, King Khalid University, Abha, Saudi Arabia*

Received 5 September 2007; accepted 17 September 2007

Available online 21 September 2007

Abstract

Needle-like nanowires, nanorods, and nanosheets containing nanowires of ZnO have been synthesized on silicon substrate by the thermal evaporation of metallic zinc powder in the presence of oxygen without the use of any catalyst or additives. It was observed that a particular type of ZnO nanostructure can be obtained in a specific temperature zone and morphology can be well controlled simply by adjusting the substrate temperature. Detailed structural analysis revealed that the formed ZnO nanostructures are single-crystalline with wurtzite hexagonal phase, grown along the [0 0 0 1] direction in preference. Raman scattering and room-temperature photoluminescence spectra showed the good crystallinity with hexagonal wurtzite phase and excellent optical properties, respectively for all the deposited ZnO nanostructures.

PACS: 68.65. +g; 78.66. Hf; 81.05. Dz; 81.10.Bk

Keywords: Nanostructures; Semiconductors; Vapor deposition; Scanning and transmission electron microscopy; X-ray diffraction

1. Introduction

Zinc oxide (ZnO) is one of the most important materials for the optoelectronic applications because of its wide band gap (3.37 eV) and high-exciton binding energy (60 meV), much larger than other semiconductor materials such as ZnSe (22 meV) and GaN (25 meV). Structurally, the ZnO has a wurtzite hexagonal phase and possesses a non-centrosymmetric structure which makes it a promising candidate for the fabrication of electromechanical coupled sensors, actuators and transducers [1,2]. Diversity in the morphologies of ZnO, synthesized by a variety of fabrication techniques was reported in the literature [3–11]. The multifariousness in the morphology of ZnO provides them an opportunity for the desirable potential applications in novel nanodevices and nanosystems. However, the shapes of ZnO nanostructures were quite dependent on growth temperature. Hence, some works related to temperature-controlled synthesis of ZnO nanostructures are reported in literature. Yao et al. reported the formation of different types of ZnO nanostructures by thermal evaporation using the ZnO and graphite powder mixture as a source material at about 1100 °C [12]. The growth of ZnO nanobelts and nanosheets at different substrate temperatures under same experimental conditions were done by Wei et al., recently [13]. They thermally evaporated the mixed powders of ZnS, SnO_2 and graphite at about 1050 °C to obtain the synthesized ZnO nanobelts and nanosheets. Zhao et al. presented the temperature dependant growth of ZnO nanostructures by the vapor-transport process using the ZnO and graphite mixture at different temperatures ranging from 900 to 1000 °C [14]. In all the reported results mentioned above, the ZnO nanostructures were grown at relatively high temperatures with good quality, but a deep level emission was also observed from the as-synthesized products which were attributed to the structural defects and impurities of the corresponding structures. However, little work has been reported for the effect of temperature on the growth of quality ZnO nanostructures at lower temperature regimes (<600 °C), which have strong ultra-violet (UV) emitting properties. It is essential to have a good optical property for the ZnO nanostruc-

* Corresponding author. Tel.: +82 63 270 2439; fax: +82 63 270 2306.
E-mail addresses: ahmadumar@chonbuk.ac.kr (A. Umar), ybhahn@chonbuk.ac.kr (Y.B. Hahn).

0925-8388/$ – see front matter © 2007 Elsevier B.V. All rights reserved.
doi:10.1016/j.jallcom.2007.09.065

tures to be utilized for the fabrication of efficient optoelectronic devices.

In this work, a temperature-controlled catalyst-free synthesis of quality ZnO nanostructures by a simple thermal evaporation process has been carried out at a modest temperature range between 480 and 600 °C. Most important, our synthesized ZnO nanostructures are exhibiting only a sharp and strong UV emission in the room-temperature photoluminescence (PL) spectra, indicating that the as-grown nanostructures have excellent optical properties with good crystallinity. This paper also presents that temperature is one of the most important factors to control the structural and optical properties of the ZnO nanostructures and by simply controlling the local substrate temperature a desired type of ZnO nanostructures can be obtained.

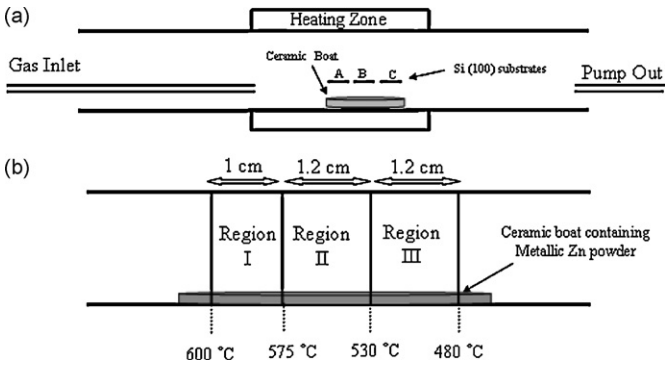

Fig. 1. (a) Schematic of the experimental setup for the fabrication of different types of ZnO nanostructures; (b) different growth zones inside the horizontal quartz tube furnace.

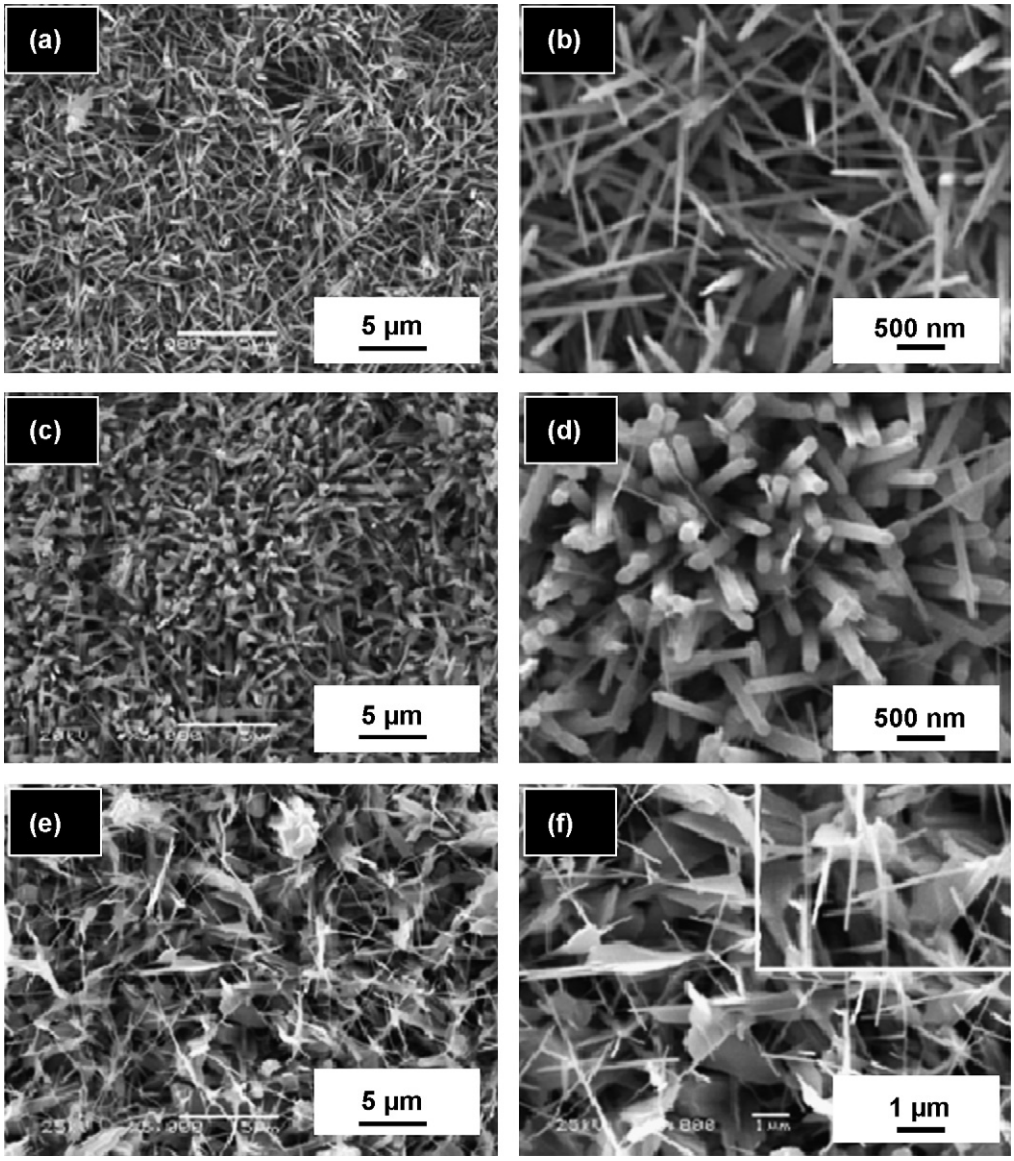

Fig. 2. Typical SEM images of the ZnO nanostructures grown on silicon substrate at different temperature regions: (a) low and (b) high magnification images of the needle like nanowires grown at position "A"; (c) low and (d) and high magnification images of ZnO nanorods formed at position "B"; (e) low and (f) and high magnification images of ZnO nanosheets containing nanowires deposited at position "C".

2. Experimental details

The synthesis of ZnO nanostructures was conducted in a conventional 50 cm long horizontal tube furnace as represented in Fig. 1(a). A ceramic boat with the length and diameter of 4 and 1.5 cm, respectively, containing the high purity metallic zinc powder (99.999%), was loaded in a quartz tube furnace. Si (1 0 0) substrate has been used to deposit ZnO nanostructures. Before loading the substrates in the reactor, they were treated for 10 min with the buffer solution to remove the native oxide layer and keenly washed with de-ionized water, acetone and methanol, and finally dried by N_2 flow. Three substrates, indicated as A, B and C were placed inside the quartz tube furnace above the ceramic boat as their polished surface faces the source material. The substrates were set in such a manner that they attain a specific temperature during the reaction (Fig. 1(a)). After this arrangement, the chamber was evacuated to 1–3 Torr using rotary vacuum pump. High purity nitrogen gas was introduced into the reactor chamber with the flow rate of 15 sccm (standard cubic centimeters per minute). The temperature of the furnace was increased to 600 °C. When the furnace temperature reached to the desired growth temperature, the oxygen gas was flowed at 30 sccm during the whole growth period. The reaction was lasted in 90 min. During the experiment, temperatures of each substrate in the quartz tube furnace were monitored with a thermal couple. The source material was placed in the temperature range of 480–600 °C, while the substrates A, B and C were placed in the temperature zones of 575–600 °C (I), 530–575 °C (II) and 480–530 °C (III), respectively (Fig. 1(b)). The deposited products were characterized by the scanning electron microscopy (SEM), transmission electron microscope (TEM), high resolution TEM (HRTEM) and X-ray diffraction (XRD) pattern measured with Cu Kα radiation. Raman scattering and room temperature photoluminescence (PL) spectroscopy measured with the Ar^+ (513.4 nm) and He–Cd (325 nm) laser line as the exciton sources were used to examine the crystal perfection and optical properties of the as-grown ZnO nanostructures, respectively.

3. Results and discussion

3.1. General morphologies and crystal structures of ZnO nanostructures

Fig. 2(a) and (b) show the low and high magnification typical SEM images of the structures deposited at substrate "A" positioned in the temperature zone I. Uniformly distributed needle-like ZnO nanowires in a high density were obtained. The typical diameters and lengths of these nanowires are in the ranges of 30–50 nm and 3–5 μm, respectively. The obtained products are randomly grown and partially aligned to the whole substrate surface with uniform density. Fig. 2(c) and (d) show the low and high magnification typical SEM images of the structures grown on substrate "B" placed in the zone II. These ZnO nanorods are uniformly grown onto the whole surface in a large quantity and almost aligned to the substrate. The average diameters and lengths of the as-grown products are in the range of 100–170 nm and 2–3 μm, respectively. The diameters of the grown nanorods are uniform through out their length and showing the clean and smooth surfaces. It is interesting to see that some of the few, very thin nanowires having the diameter of 15–25 nm with the length of 4–6 μm were observed from the sample which seemed that they were originated from the facets of nanorods. The low and high magnification typical SEM images of the products grown on substrate "C" placed in the zone III were shown in Fig. 2(e) and (f). ZnO nanowires attached with the ZnO nanosheets were observed. Interestingly, the obtained nanowires are rooted in the outer surfaces of the nanosheets. The average thicknesses of these ZnO nanosheets are in the range of 50–60 nm with several micrometers wide. The diameters and lengths of the originated nanowires are in the range of 20–30 nm and 6–8 μm, respectively, and are exhibiting smooth surfaces with uniform diameter passim their length. All the grown ZnO nanostructures reported here have a good reproducibility under the same experimental setup and conditions employed for this work.

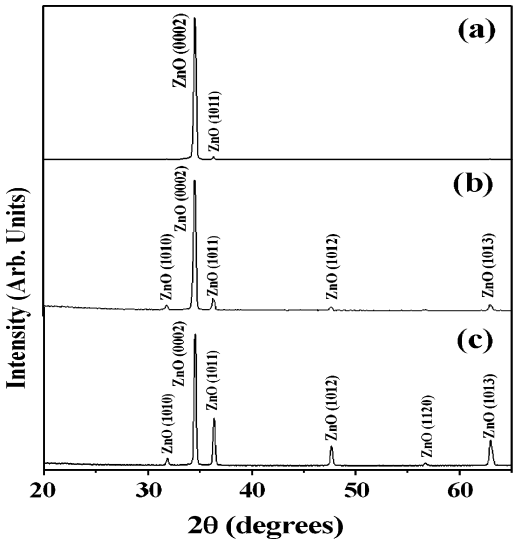

Fig. 3. XRD patterns of different ZnO nanostructures grown on positions (a) A, (b) B, and (c) C placed in the different temperature regions.

Fig. 3 shows the typical XRD patterns for the ZnO nanostructures deposited at different temperature zones. The presence of high intensity, strong and sharp peak at 34.2° assigned to be as ZnO (0 0 0 2), in all the spectra, indicated that the grown nanostructures are preferentially grown in *c*-axis direction. No additional peaks from the unreacted zinc or other impurities were found in the spectra. Overall, due to the stronger in intensity and the narrower in spectral width of ZnO (0 0 0 2) peak as compared to the other (1 0 1 0) and (1 0 1 1) peaks confirm that the as-grown nanostructures are highly crystalline and preferentially oriented in the *c*-axis direction.

For the further detailed structural characterization by TEM, the needle-like ZnO nanowires grown in the zone I was chosen. Fig. 4(a) shows the close view of the root portion of the ZnO nanowire. The TEM image confirms that the typical diameter of the nanowires at its root lies in between 30 and 50 nm and decreases with increasing its length. The corresponding SAED pattern of the root portion shows that the needle-like ZnO nanowire is single crystalline, grown along the *c*-axis direction (inset of (a)). Fig. 4(b) demonstrates the tip portion of the nanowire which clearly indicates that the nanowires has a sharp tip with the wide root and its diameter decreases gradually from root to the tip. These low magnification images indicate that they have smooth and clean surfaces without any structural defects. Fig. 4(c) shows the high resolution TEM (HRTEM) image of circled portion of the single crystalline nanowire shown in Fig. 4(b), which confirms that the as-grown nanowires are structurally uniform and free from any type of noticeable defects such as dislocations and stack-

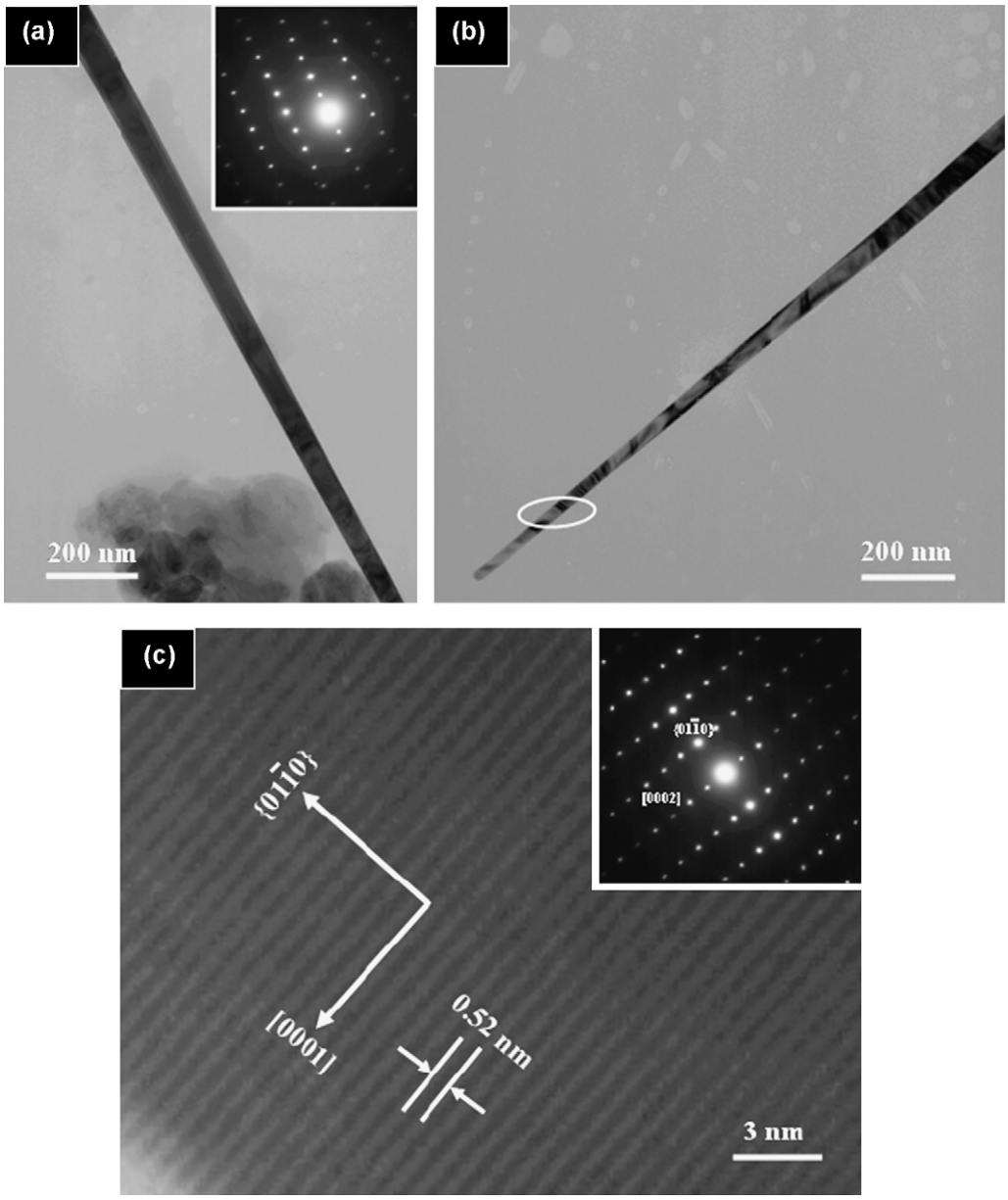

Fig. 4. Low resolution TEM images of (a) root and (b) tip portion of the needle-like ZnO nanowires grown at position "A" and the corresponding SAED pattern of the root portion (inset); (c) high resolution TEM images of circled portion of tip of the ZnO nanowire shown in (b) and its corresponding SAED pattern (inset).

ing faults. The lattice spacing of about 0.52 nm corresponds to the *d*-spacing of (0 0 0 1) planes verified the wurtzite hexagonal structure for the grown products. The SAED pattern of this same circled area projected along the [2 $\bar{1}$ $\bar{1}$ 0] zone axis is fully consistent with the HRTEM observation (inset (c)) and confirms the single crystallinity and *c*-axis growth direction for the as-grown nanowires.

3.2. Detailed optical properties of the ZnO nanostructures

Fig. 5 shows the Raman scattering of the ZnO nanostructures grown at the different temperature zones. The appearance of a high intensity, dominated, strong and sharp peak at 437 cm^{-1}, over other peaks except silicon substrate, is attributed to be as the Raman active optical phonon E_2 mode for the wurtzite hexagonal phase of the ZnO [15]. The presences of Raman active E_2 mode in all the spectra affirm that all the grown products on different substrates (from A to C) have wurtzite hexagonal structures [15]. Two weak peaks in the range of 330–331 and 378–379 cm^{-1} are also observed, which are assigned to be as E_{2H}–E_{2L} (multi phonon process) and A_{1T} modes, respectively [15,16]. No peaks for E_{1L} mode are observed in all the spectra. The appearance of E_{1L} mode in the Raman spectra is considered due to the crystal structural defects and impurities such as oxygen vacancies, zinc interstitials, etc. [17,18]. Hence, the appearance of high intensity, sharp and dominated E_2 mode with the absence of E_{1L} peak in the Raman spectra substantiates that the ZnO nanostructures grown in different temperature zones are good in crystal quality with hexagonal wurtzite crystal structure.

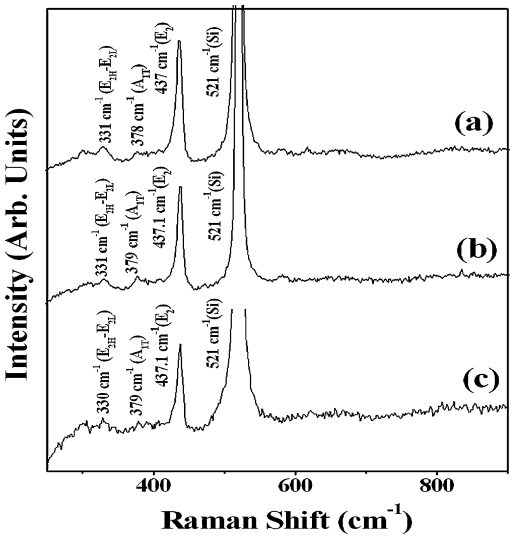

Fig. 5. Raman scattering of different ZnO nanostructures grown on the substrate (a) A, (b) B and (c) C placed in the different temperature regions.

Fig. 6 shows the corresponding room temperature PL spectra for the ZnO nanostructures grown on the substrates of A, B and C. All our synthesized ZnO nanostructures at different temperature zones exhibit only a sharp and strong peak in the UV emission at 379 nm while no other peak is detected. The UV emission, known as near-band-edge emission (NBE) is originated from the recombination of free-exciton through an exciton–exciton collision process, while the green emission, also known as deep-level emission appears due to the radial recombination of a photo-generated hole with a singly ionized charge state of the specific defect (oxygen vacancies) [8,19]. In general, it is known that the green emission is caused by structural defects, oxygen vacancies, interstitials of zinc, impurities, etc. [9,20]. Therefore, the appearance of a sharp and strong intensity NBE emission and no green emission indicate that the as-grown ZnO nanostructures have a good crystal quality with excellent optical properties. These PL results are consistent with the Raman study. Due to the excellent optical properties of the grown structures they are highly applicable for the fabrication of nano-optoelectronic devices in near future.

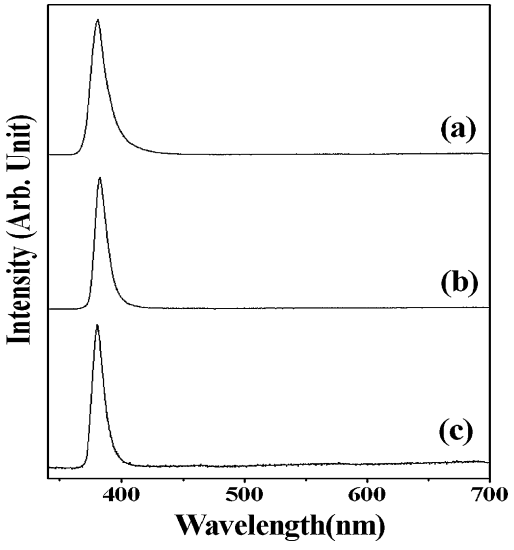

Fig. 6. Room temperature PL spectra of different ZnO nanostructures grown on the substrate (a) A, (b) B and (c) C placed in the different temperature regions.

3.3. Growth mechanism of the ZnO nanostructures

On the basis of obtained results, we can reason out the possible growth steps for the formation of different types of ZnO nanostructures in the different temperature zones inside a single reactor. Neither a metal catalyst was used for synthesis nor detected from the grown products; hence a vapor–solid (VS) mechanism [6,9,16] has been referred for the grown nanostructures in our synthesis rather to the widely used conventional vapor–liquid–solid (VLS) growth process [21]. The ZnO nanostructures in this synthesis were formed onto the substrate through a simple chemical reaction:

$$Zn\,(g) + 1/2O_2\,(g) \rightarrow ZnO\,(s)$$

In our experimental condition, as the boat containing the metallic zinc powder was arranged in the temperature ranges between 480 and 600 °C, which provide sufficient temperature for the evaporation of metallic zinc powder (m.p. of Zn = 419 °C). The growth of ZnO nanostructures can be divided into two parts, i.e. nucleation and growth. Initially, when the temperature of the furnace reaches to the desired value above the melting point of zinc, the zinc atoms start to evaporate from the metallic zinc powder and deposit onto the substrates placed above the source material. The substrates are then coated with the metallic zinc layer but when the oxygen is introduced into the reactor, the deposited zinc starts to be oxidized, arranging with proper cation–anion coordination and forming the ZnO nanoclusters on to the substrates. The newly coming molecules (zinc atoms and oxygen), from the continuous supply of the reactants, may start to deposit onto the previously formed ZnO nanoclusters, which leads the growth of various nanostructure. The zinc and oxygen molecules arranged in such a manner that the lattice fringes of the structures become continuous without any grain boundary and crystal defects. It is evident from the HRTEM image (Fig. 4(c)) that no stacking fault or any kind of structural defects exist in the deposited nanostructures. Structurally, the ZnO is a wurtzite polar crystal containing the O^{2-} ions which arranged in hexagonal closest packing while the Zn^{2+} ions lying within a tetrahedral group of four oxygen ions. So the zinc and oxygen ions are arranged in a fourfold tetrahedral coordinated manner and stacked along the *c*-axis, alternatively. ZnO has positively charged (0 0 0 1)-Zn terminated and negatively charged (0 0 0 1)-O polar surfaces, in which the (0 0 0 1)-Zn surface is chemically active for the growth of nanostructures while (0 0 0 1)-O is inert. According to the lowest energy principle, the surface energy of the (0 0 0 2) facet is lowest hence the growth velocity along the [0 0 0 1] is faster [16]. Therefore the growth along the [0 0 0 1] direction is a dominated growth facet compared to other growth facets. In our synthesized ZnO nanostructures reported here are exhibiting a preferential growth in the [0 0 0 1] direction which was

confirmed by the HRTEM, XRD and SAED patterns. Additionally, it is also observed that the substrate temperature play an important role for the deposition of different kinds of nanostructures in a single reactor. Our experimental results show that particular type of nanostructures can be obtained in a specific temperature zone and it may be possible to tailor a specific type of ZnO nanostructure by the tuning of the reaction temperature [12–15]. However, it is not completely understood yet that why the substrate temperature has such a great influence onto the morphologies of the deposited products. Finally, more studies are needed to understand the complete growth process for the formation of different types of ZnO nanostructures. Further experiments are underway and will be reported in another article.

4. Conclusions

In summary, we have successfully synthesized different types of ZnO nanostructures such as needle-shaped nanowires, nanorods and nanosheets containing the nanowires at the temperature range between 480 and 600 °C by the simple thermal evaporation approach using the metallic zinc powder in the presence of oxygen without the use of catalyst or additives. It is observed from our experimental results that the local substrate temperature is an important parameter for the growth of nanostructures and a particular type of ZnO nanostructure can be grown in a specific temperature zone. The detailed structural studies confirm the single crystallinity with a hexagonal wurtzite phase and preferential growth along the [0 0 0 1] direction for the deposited ZnO nanostructures. The appearance of high intensity, sharp and dominated E_2 mode with the absence of E_{1L} mode in the Raman spectra indicates that the as-grown ZnO nanostructures are good in crystal quality with the wurtzite hexagonal structure. Additionally, sharp and strong UV emissions with no green emission in the room-temperature PL spectra indicate that our grown ZnO nanostructures have excellent optical properties and are promising for the fabrication of efficient nano-optoelectronic devices in near future.

Acknowledgements

This work was supported by the Korea Research Foundation grant (KRF-2005-005-J07502) (MOEHRD) and by the Brain Korea 21 project in 2007. Authors wish to thanks Mr. T.S. Bae and J.C. Lim, KBSI, Jeonju branch, and Mr. Jong-Gyun Kang, Centre for University Research Facility for taking good quality SEM and TEM images, respectively.

References

[1] A. Kuoni, R. Holzherr, M. Boillat, N.F. de Rooij, J. Micromech. Microeng. 13 (2003) S103.
[2] Z.R. Dai, Z.W. Pan, Z.L. Wang, Adv. Funct. Mater. 13 (2003) 9.
[3] A. Sekar, S.H. Kim, A. Umar, Y.B. Hahn, J. Cryst. Growth 277 (2005) 471.
[4] A. Umar, S.H. Kim, Y.S. Lee, K.S. Nahm, Y.B. Hahn, J. Cryst. Growth 282 (2005) 131.
[5] A. Umar, E.K. Suh, Y.B. Hahn, Solid State Commun. 139 (2006) 447.
[6] A. Umar, H.W. Ra, J.P. Jeong, E.K. Suh, Y.B. Hahn, Korean J. Chem. Eng. 23 (2003) 499.
[7] X.Y. Kong, Y. Ding, R.S. Yang, Z.L. Wang, Science 303 (2004) 1348.
[8] A. Umar, B. Karunagaran, E.K. Suh, Y.B. Hahn, Nanotechnology 17 (2006) 4072.
[9] A. Umar, Y.B. Hahn, Nanotechnology 17 (2006) 2174.
[10] A. Umar, S. Lee, Y.S. Lee, K.S. Nahm, Y.B. Hahn, J. Cryst. Growth 277 (2005) 479.
[11] A. Umar, S. Lee, Y.H. Im, Y.B. Hahn, Nanotechnology 16 (2005) 2462.
[12] B.D. Yao, Y.F. Chen, N. Wang, Appl. Phys. Lett. 81 (2002) 757.
[13] Q. Wei, G. Meng, X. An, Y. Hao, L. Zhang, Nanotechnology 16 (2005) 2561.
[14] D. Zhao, C. Andreazza, P. Andreazza, J. Ma, Y. Liu, D. Shen, Chem. Phys. Lett. 399 (2004) 522.
[15] Y.J. Xing, Z.H. Xi, Z.Q. Xue, X.D. Zhang, J.H. Song, R.M. Wang, J. Xu, Y. Song, S.L. Zhang, D.P. Yu, Appl. Phys. Lett. 83 (2003) 1689.
[16] A. Umar, Y.B. Hahn, Appl. Phys. Lett. 88 (2006) 173120.
[17] M. Rajalaxmi, A.K. Arora, B.S. Bendre, S. Mahamuni, J. Appl. Phys. 87 (2000) 2445.
[18] M. Tzolov, N. Tzenov, D.D. Malinovska, M. Kalitzova, C. Pizzuto, G. Vitali, G. Zollo, I. Ivanov, Thin Solid Films 379 (2000) 28.
[19] K. Vanheusden, W.L. Warren, C.H. Seager, D.R. Tallant, J.A. Voigt, B.E. Gnade, J. Appl. Phys. 79 (1996) 7983.
[20] A.B. Djurišić, Y.H. Leung, W.C.H. Choy, K.W. Cheah, W.K. Chan, Appl. Phys. Lett. 84 (2004) 2635.
[21] A. Umar, J.P. Jeong, E.K. Suh, Y.B. Hahn, Korean J. Chem. Eng. 23 (2006) 860.